Hindawi Publishing Corporation
EURASIP Journal on Wireless Communications and Networking
Volume 2010, Article ID 414927, 14 pages
doi:10.1155/2010/414927

Research Article

On the Evaluation of MB-OFDM UWB Interference Effects on a WiMAX Receiver

Eduardo Cano, Alberto Rabbachin, Detlef Fuehrer, and Joaquim Fortuny

Institute for the Protection and Security of the Citizen, Joint Research Centre, European Commission, Ispra, 21027 Varese, Italy

Correspondence should be addressed to Eduardo Cano, eduardo.cano@jrc.ec.europa.eu

Received 1 November 2009; Revised 20 April 2010; Accepted 6 July 2010

Academic Editor: Yan Xin

The European Commission has recently adopted specific power spectral density masks for ultra wideband (UWB) devices, with detect and avoid capabilities, for coexistence with licensed standards. Under these regulations, a novel approach for analyzing the UWB interference effects on the WiMAX downlink is provided in this paper by means of a novel theoretical computation of the bit error rate (BER), simulation results, and measurements in a conducted modality. New analytical BER expressions for both uncoded and coded WiMAX systems, impaired by a single multiband-OFDM (MB-OFDM) UWB interference signal, are obtained in this paper for a Rayleigh fading channel. The BER is expressed in terms of the characteristic function of the interference signal. The maximum permissible interference levels and the signal-to-interference (SIR) values, which allow the UWB interference effects to be considered negligible, are estimated in this paper from simulation and measurement results. The analysis considers a WiMAX receiver operating at its minimum sensitivity level. The BER, the symbol error probability (SEP), and the error vector magnitude (EVM) of the WiMAX link are the metrics employed to characterize the interference effects for both frequency hopping and nonfrequency hopping UWB interferers.

1. Introduction

The demand for reliable, fast, and low-cost data communications services for all types of wireless applications and environments has increased rapidly in the last few years. Often, different types of wireless networks coexist in the same area and share the communications channel. In such situations, if appropriate mitigation techniques are not applied, wireless signals coming from different sources could interfere with each other causing a considerable degradation in system performance. The coexistence scenario analyzed in this work corresponds to the case of a single ultra wideband (UWB) transmitter operating at the same frequency band as a WiMAX receiver. UWB technology is established as a viable candidate for future wireless personal area networks (WPANs) that require the processing of information with low-power sources at very high speeds across short distances (order of 10 m) [1]. Alternatively, WiMAX systems, which are derived from the IEEE 802.16 air interface standards [2, 3], allow for high-speed broadband connectivity in cellular point-to-multipoint wireless metropolitan area networks (WMAN) of wider range (order of 5 Km).

The Federal Communications Commission (FCC) in the US approved the use of UWB technology for commercial applications under part 15 of its regulations in February 2002 [4]. The FCC report and order defined UWB as a signal with bandwidth to central frequency ratio greater than 20% or, alternatively, with a −10 dB bandwidth exceeding 500 MHz in the frequency range of 3.1–10.6 GHz. The FCC permits UWB devices to operate on an unlicensed basis following restrictive power spectral masks for both indoor and outdoor environments. A maximum mean effective isotropic radiated power (EIRP) spectral density of −41.3 dBm/MHz is established over all the 7.5 GHz operation bandwidth. Under these initial conditions, UWB devices can cause harmful interference to primary services operating simultaneously in their vicinity. This is the scenario under which WiMAX systems operate at 3.5 GHz in Europe.

On February 21, 2007 the European Commission issued its Decision 2007/131/EC, which regulates the use of radio spectrum for equipment using UWB in a harmonized manner in the European Community [5]. The European regulations for UWB are based on the former FCC indoor mask with considerable restrictions on the EIRP levels

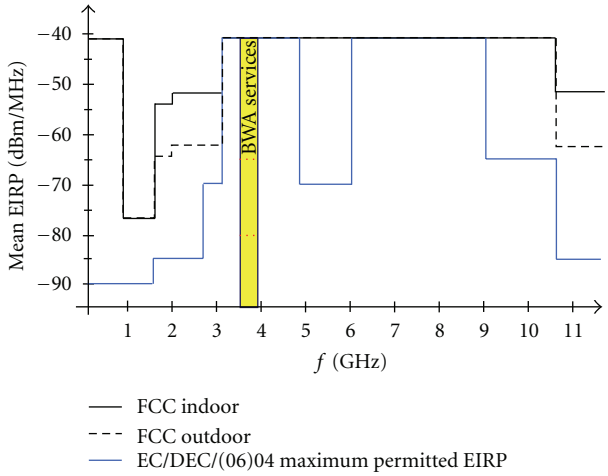

Figure 1: EIRP masks for FCC indoor, FCC outdoor, and EU regulations.

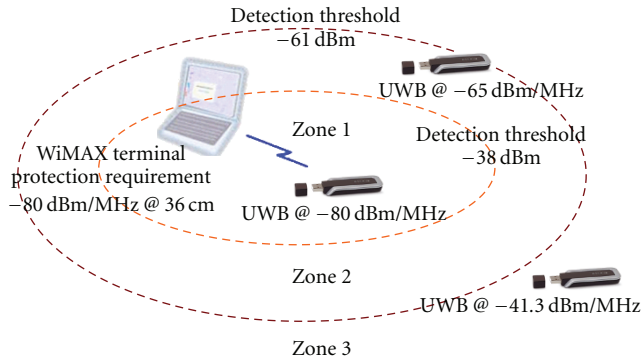

Figure 2: Protection zones associated with DAA in the 3.5 GHz band.

in specific bands as illustrated in Figure 1. In particular, detect and avoid (DAA) or low duty cycle (LDC) mitigation techniques are imposed in the band 3.1–4.8 GHz to protect licensed broadband wireless access (BWA) services [6]. The DAA mechanism is based on the definition of three zones for which an appropriate maximum mean EIRP spectral density is authorized. In DAA mode, the UWB device detects and estimates the power level of the WiMAX service and dynamically adapts its EIRP level depending on the zone of operation. This coexistence operation is reflected in Figure 2, in which the power threshold levels are between zones −38 dBm and −61 dBm. The maximum mean EIRP spectral density levels are −41.3 dBm/MHz, −65 dBm/MHz and −80 dBm/MHz for zones 1, 2, and 3, respectively.

The objective of this work is to evaluate the interference effects caused by a UWB transmitter, compliant with the EU DAA regulations and which follows the multiband OFDM (MB-OFDM) approach [7], on a WiMAX receiver by means of theoretical analysis, simulations, and experimental results.

Several studies that evaluate the coexistence between WiMAX systems and UWB devices with DAA functionality have been carried out in the literature [8–14]. However, there is a lack of published work that validates the theoretical findings in practical implementations and viceversa. In an analytical approach, novel expressions for the bit error rate (BER) for uncoded/coded WiMAX systems are presented in this paper, based on the statistical characterization of the MB-OFDM UWB interference. A similar approach for obtaining the BER in coded systems can be found in [15, 16] and for uncoded systems in [17]. In contrast to the aforementioned works, a novel closed form of the BER for the WiMAX link in the presence of Rayleigh fading is obtained by means of computing the characteristic function of the MB-OFDM interference signal without using numerical integration methods. Furthermore, the analytical BER functions obtained in this paper are expressed in terms of the maximum allowable signal-to-interference (SIR) levels measured at the input of the WiMAX victim receiver. In the measurement study, the impact of the UWB interference on the WiMAX receiver is analyzed in a conducted modality using the error vector magnitude (EVM) and the symbol error probability (SEP) as evaluation metrics.

The remainder of the paper is organized as follows. Section 2 provides a detailed description of the WiMAX communications link and the processing of the received signal, as well as the model of the MB-OFDM UWB interference. In Section 3, novel analytical expressions for the BER for both uncoded and coded WiMAX systems in the presence of a single MB-OFDM UWB interference are presented, along with a link budget analysis to estimate the interference margins. Simulation and experimental results of the most relevant scenarios, in the context of interference, are presented in Sections 4 and 5, respectively. Finally, conclusions are presented in Section 6.

Notation. In this paper, $(\cdot)^*$, $\mathbb{E}\{\cdot\}$, $\Re\{\cdot\}$, $\Im\{\cdot\}$, $\mathbb{P}\{\cdot\}$, and $\otimes$ denote complex conjugation, statistical expectation, the real part of a complex number, the imaginary part of a complex number, the probability of an event, and the convolution operator, respectively.

2. System Model

The system model consists of a WiMAX base station, transmitting data information to a WiMAX customer-premises equipment (CPE) receiver, and a MB-OFDM UWB transmitter that follows the ECMA-368 standard [18].

2.1. WiMAX System. The WiMAX system employed in this work follows the specifications of the IEEE 802.16-2004 for fixed wireless access networks [2]. This system is based on OFDM with $N_s^w = 256$ subcarriers, of which $N_d^w = 192$ are used for data processing, $N_g^w = 56$ are nulled for guard band protection and $N_p^w = 8$ are designated for channel estimation purposes.

A robust forward error control (FEC) technique based on a two-stage process is employed in the standard. This concatenated code is constructed by using an outer Reed-Solomon (RS) code and an inner punctured convolutional code (CC). The CC encoder corrects independent bit errors,

while the RS code corrects burst errors at the byte level. Four modulation schemes are specified in the IEEE 802.16-2004 standard for both downlink (DL) and uplink (UL) transmissions. These modulation schemes are binary phase shift keying (BPSK), quaternary phase shift keying (QPSK) and M-ary quadrature amplitude modulation (QAM) with modulation orders $M = 16$ and $M = 64$. The PHY specifies seven burst profiles as a result of combining modulations and FEC rates that can be assigned to both CPEs and base stations. The selection of an appropriate modulation-code combination depends on the required performance, taking into consideration tradeoffs between data rate and system robustness. Two modulation-coding formats, QPSK and 64-QAM with overall coding rates $R_c^w = 1/2$ and $R_c^w = 3/4$, respectively, are used in this work.

A high-level representation of the WiMAX system is depicted in Figure 3. Each OFDM transmitted symbol is generated from a subset of data information bits, represented by the vector $\mathbf{b}$ of length $L_B = \log_2(M)N_d^w R_c^w - 8$. The encoded bits are interleaved as $\mathbf{c}^\pi = \prod\{\mathbf{c}\}$ prior to going through a modulation memory-less mapper, $\widetilde{\mathbf{x}} = \mathcal{M}\{\mathbf{c}^\pi\}$ of length $L_x = N_d^w$, which follows a Gray-labeled constellation. The elements of the complex modulated signal are mapped into the data subcarriers and the OFDM data symbol is formed by including the pilot and guard values into the correspondent subcarriers. Subsequently, the inverse fast fourier transform (IFFT) is applied to obtain a temporal vector of N_s^w samples, $\mathbf{x}_\nu \triangleq [x_{0,\nu}, x_{1,\nu}, \ldots, x_{N_s^w-1,\nu}]$, where ν is the symbol index. The discrete baseband OFDM symbol is generated by appending a cyclic prefix of N_{cp}^w samples and duration T_{cp}^w to the IFFT symbol. The transmitted baseband OFDM signal is computed as

$$s(t) = \sum_{\nu=-\infty}^{+\infty} \sum_{k=0}^{N_s^w-1} x_{k,\nu} w_k\left(t - \nu T_s^w\right), \tag{1}$$

where $w_k(t) \triangleq e^{j2\pi\Delta f_w kt} p(t)$ is the kth OFDM subcarrier waveform, $\Delta f_w = W_w/N_s^w$ is the subcarrier spacing and W_w is the bandwidth of the WiMAX signal. The basis function $p(t)$ is an ideal rectangular pulse of unitary energy and duration equal to the symbol time $T_s^w = 1/\Delta f_w + T_{\text{cp}}^w$. The RF transmitted signal is obtained by upconverting the baseband signal to the frequency $f_w = 3.5$ GHz, as $s_{\text{RF}}(t) = s(t)e^{j2\pi f_w t}$.

The radiated signal $s_{\text{RF}}(t)$ is transmitted over a multipath fading channel with impulse response $h^w(t)$, which is assumed to be shorter than T_{cp}^w in order to avoid intersymbol interference. The channel impulse response is considered to be time invariant during the transmission of one packet. The received signal $r_{\text{RF}}(t)$ is impaired by additive white Gaussian noise (AWGN) $n(t)$ and the MB-OFDM UWB interference signal. Thus, the received signal, after applying the bandpass filtering and downconversion to baseband, is given by

$$r(t) = s(t) \otimes h^w(t) + n(t) + i_R(t), \tag{2}$$

where $i_R(t)$ is the interference signal contribution measured at the WiMAX receiver.

The baseband processing chain consists of low-pass filtering, sampling, and FFT mechanism that can be equivalently modeled as a bank of N_s^w filters matched to the function $w_k(t)$ followed by a sampling process [19]. The impulse response of the subcarrier matching filter is given in (3) for $0 \le k \le N_s^w - 1$ as

$$\phi_k(t) = \begin{cases} w_k^*(-t)e^{-j\eta_k} & \text{if } -\dfrac{1}{\Delta f_{\text{w}}} \le t \le 0, \\ 0, & \text{else,} \end{cases} \tag{3}$$

where η_k represents the frequency-domain channel phase estimated at the coherent WiMAX receiver and it is uniformly distributed on $[0, 2\pi)$. Perfect channel state information is assumed in this paper.

Without loss of generality, the transmission of symbol index $\nu = 0$ is considered in the following analysis. The output of the kth correlated signal is sampled at $kT_w = k/\Delta f_w$ in order to obtain the statistic variable as

$$r_k = \left(r(t) \otimes \phi_k(t)\right)|_{t=kT_w} = s_k + n_k + i_k, \tag{4}$$

where s_k, n_k, and i_k are the data information contribution, the AWGN component and the interference term received at the subcarrier k, respectively. Due to the orthogonality factor between correlation function and subcarrier waveform, the information term can be expressed as $s_k = G_k x_{k,0}$, where G_k is the frequency-domain channel gain and follows a Rayleigh distribution. The interference component can be generally computed as

$$\begin{aligned} i_k &= \int_{\langle T_w \rangle} i_R(t)\phi_k(t)dt \\ &= \int_{\langle T_w \rangle} \left(h^u(t) \otimes i(t-\tau)e^{j2\pi f_{u,w}t}\right)\phi_k(t)dt, \end{aligned} \tag{5}$$

where $i(t)$ is the baseband UWB interference signal and $h^u(t)$ is the channel impulse response of the filtered UWB interference of duration T_s^w. The parameters $f_{u,w}$ and τ in (5) are the frequency offset of the UWB interference relative to the WiMAX center frequency and the time delay of the UWB interference measured at the input of the WiMAX receiver and uniformly distributed on $[0, T_s^w)$, respectively.

2.2. MB-OFDM UWB Interference. The interferer system employed in this work is modeled as a MB-OFDM UWB transmitter, which follows the ECMA-368 standard [18]. In MB-OFDM UWB systems, the available 7.5 GHz bandwidth is divided into fourteen subbands, each having a bandwidth of 528 MHz. These subbands are grouped into six band groups (BG1-BG6) of three subbands each, except BG5 which has two subbands. The center frequency of the mth subband is defined as $f_u = 2904 + m528$ MHz.

The MB-UWB OFDM signal is organized in packets that are sequentially composed of preamble, header, and payload data symbols. The payload data can be transmitted at different data rates. The data rate values R_b^u fixed by the standard, are 53.3, 80, 106.7, 160, 200, 320, 400, and 480 Mbps. These data rate values are obtained by selecting different combinations of modulation schemes and coding rates. The coding rate value is obtained at the output of

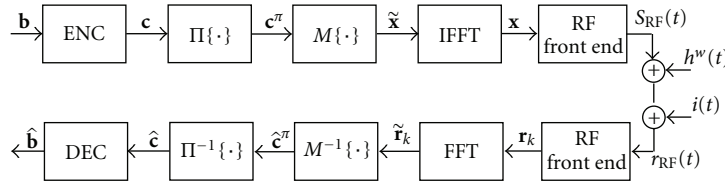

Figure 3: High-level block diagram of the WiMAX signal processing chain.

a puncturing block with values $R_c^u = 1/2$, 1/3, 3/4, and 5/8. Two different modulation schemes are implemented; a QPSK scheme for data rates of 200 Mbps and below and a dual carrier modulation (DCM) scheme that is used for higher data rate values.

The header and the payload data symbols are generated by using an OFDM technique with $N_s^u = 128$ subcarriers of which $N_d^u = 100$ are data subcarriers, $N_p^u = 12$ are pilots, $N_g^u = 10$ are for guard protection and the rest are nulled.

The time-domain samples of the preamble, header, and data payload are concatenated to generate the baseband discrete packet and then passed through a digital-to-analog converter (DAC). The continuous signal is up-converted to the RF frequencies by using a time-frequency code (TFC) pattern that allows frequency-hopping capabilities over the different bands that integrate a band group. Among all of the ten different TFC codes, TFC1, and TFC5 applied in BG1 are of particular interest in this paper, since they reflect the effects of the hopping and nonhopping MB-OFDM UWB interference signal, respectively, on the WiMAX band.

The baseband MB-OFDM UWB interference signal is given by

$$i(t) = \sum_{l=-\infty}^{+\infty} \sum_{p=0}^{N_s^u-1} \sqrt{P_U} d_{p,l} z_p(t - lT_s^u), \tag{6}$$

where $d_{p,l}$ is the modulation value of the symbol l mapped into the subcarrier p and P_U is the transmitted power of the interference signal. Similarly, the function $z_p(t)$ in (6) is obtained as $z_p(t) \triangleq e^{j2\pi\Delta f_u pt} q(t)$, where $q(t)$ is the basis function modeled as a rectangular pulse of unitary energy with duration equal to the symbol time $T_s^u = 1/\Delta f_u + T_{\text{cp}}^u$. The following parameters $\Delta f_u = W_u/N_s^u$, W_u and T_{cp}^u are the subcarrier spacing, the bandwidth of the UWB signal, and the cyclic prefix duration, respectively.

Furthermore, the expression of the sampled interference contribution obtained at the WiMAX receiver can be computed by substituting (6) into (5) to obtain

$$i_k = \sum_{l=-\infty}^{+\infty} \sum_{p=0}^{N_s^u-1} h_p e^{j(\alpha_p - \eta_k)} d_{p,l} c_{k,p,l}, \tag{7}$$

where α_p is a random variable uniformly distributed on $[0, 2\pi)$ and h_p is the frequency-channel amplitude of the UWB pth subcarrier. It is assumed that the frequency response of the UWB channel is constant over the WiMAX subcarrier frequency band. The parameter $c_{k,p,l}$ in (7) can be calculated as

$$c_{k,p,l} = \int_{\langle T_w \rangle} \sqrt{P_U} z_p(t - lT_s^u - \tau) w_k^*(t) e^{j2\pi f_{u,w} t} dt. \tag{8}$$

This integration can be solved in closed form [17] leading to

$$c_{k,p,l} = \left(\frac{e^{j2\pi(\Delta f_u p - \Delta f_w k + f_{u,w})I} - e^{j2\pi(\Delta f_u p - \Delta f_w k + f_{u,w})J}}{j2\pi(\Delta f_u p - \Delta f_w k + f_{u,w})\sqrt{T_w T_u}} \right) \times \sqrt{P_U} e^{j2\pi(\Delta f_w k T_{\text{cp}}^w - \Delta f_u p T_{\text{cp}}^u)}, \tag{9}$$

where T_u is the symbol duration of the MB-OFDM UWB signal without appending the cyclic prefix, $I = \max(T_{\text{cp}}^w, lT_s^u + \tau)$ and $J = \min(T_s^w, (l+1)T_s^u + \tau)$.

3. Performance Analysis

In this section, analytical BER expressions for the WiMAX link, impaired by MB-OFDM UWB interference, are provided for uncoded (Section 3.1) and coded (Section 3.2) systems using QPSK and M-QAM modulation formats. Subsequently, the minimum required SIR values, which allow the interference to be considered negligible, and the minimum distance among DAA protection zones are estimated in Section 3.3.

3.1. BER Performance for Uncoded WiMAX Systems. Considering the situation in which a data symbol $\tilde{x}_0$ is transmitted by the WiMAX base station, the general expression of the symbol error probability, conditioned to $\tilde{x}_0$, is obtained by applying the inversion theorem [20] as

$$\mathbb{P}\{r_k < d_{\tilde{x}_0} \mid \psi_{r_k}(s)\} = \frac{1}{2} + \frac{1}{2\pi} \int_0^{+\infty} \frac{e^{jsd_{\tilde{x}_0}} \psi_{r_k}(-s) - e^{-jsd_{\tilde{x}_0}} \psi_{r_k}(s)}{js} ds, \tag{10}$$

where $d_{\tilde{x}_0}$ is the threshold value of the symbol $\tilde{x}_0$ with respect to the other symbols of the constellation and $\psi_{r_k}(s)$ is the characteristic function (CF) of the decision variable r_k expressed in (4). The BER is computed in closed form by calculating the CF of the decision variable as follows:

$$\psi_{r_k}^{(m)}(s) = \mathbb{E}\left\{e^{-jsr_k}\right\} = \begin{cases} \psi_{G_k}(s)\psi_{n_k}(s)\psi_{i_k}(s), & m = 1, \\ \psi_{G_k}(s)\psi_{n_k}(s), & m = 2, \end{cases} \tag{11}$$

where G_k, i_k, and n_k are independent variables. Note that $\psi_{r_k}^{(2)}(s)$ accounts for the interference-free situation.

In the following analysis, the CF of the decision variable is obtained by calculating the CF of the individual contributions which are fading of the primary signal, noise, and MB-OFDM UWB interference terms.

The parameter G_k is a Rayleigh random variable and its CF [21, page 45] can be obtained as

$$\psi_{G_k}(s) = -e^{-a_g}\sum_{l=0}^{\infty}\frac{a_g^l}{(2l-1)l!} + j\sqrt{\frac{\pi}{2}}s\sigma_g e^{-s^2\sigma_g^2/2}, \tag{12}$$

where $a_g = (1/2)s^2\sigma_g^2$, and σ_g^2 is the variance of G_k.

Furthermore, the CF of the Gaussian random variable can be easily calculated as

$$\psi_{n_k}(s) = e^{(-s^2\sigma_n^2)/2}, \tag{13}$$

where $\sigma_n^2 = \mathbb{E}\{n_k^2\} = N_0/2$ is the variance of n_k, which is independent of k, and N_0 is the noise power spectral density.

Finally, the CF of i_k in (7) is obtained by conditioning its real part to the variables τ, α_p, and h_p to give

$$\begin{aligned}\psi_{i_k}\left(s \mid \tau, \alpha_p, h_p\right) &= \mathbb{E}\left\{e^{-js\Re\{i_k\}} \mid \tau, \alpha_p, h_p\right\} \\ &= \prod_{l=-\infty}^{+\infty}\prod_{p=0}^{N_s^u-1}\mathbb{E}\left\{e^{-js\Re\{h_p e^{j(\alpha_p-\eta_k)}d_{p,l}c_{k,p,l}\}}\right\}.\end{aligned} \tag{14}$$

The variables h_p and η_p are independent of the subcarrier index, since only very few UWB subcarriers contribute to the interference component within the narrowband WiMAX channel. In addition, the differential phase in (14) can be expressed as $\tilde{\alpha} = \alpha - \eta_k$ and $\tilde{\alpha}$ is a uniformly distributed variable on $[0, 2\pi)$. It is also assumed that changing the value of τ does not affect the expectation result; therefore, $c_{k,p,l}$ is considered deterministic. Thus, the CF of the interference term is simplified to the following expression:

$$\begin{aligned}\psi_{i_k}(s \mid \tilde{\alpha}, h) = \prod_{l=-\infty}^{+\infty}\prod_{p=0}^{N_s^u-1}&\cosh\left(s\Re\left\{he^{j\tilde{\alpha}}c_{k,p,l}\right\}\right) \\ &\times\cosh\left(s\Im\left\{he^{j\tilde{\alpha}}c_{k,p,l}\right\}\right).\end{aligned} \tag{15}$$

The expression of $\psi_{i_k}(s)$ can be calculated from (15) by taking the expectations of $\tilde{\alpha}$ and h. However, a closed form expression of the BER cannot be obtained by using this procedure. In this case, the average BER would be computed using numerical integrations that require averaging over all possible realizations of $\tilde{\alpha}$ and the Rayleigh variable h. However, this approach requires large computational calculations. The objective of this work is to obtain an approximated closed form expression of $\psi_{i_k}(s)$ as follows. Initially, the real part of the interference term in (7) is expressed as

$$\begin{aligned}\Re\{i_k\} &\approx \Re\left\{he^{j\tilde{\alpha}}\sum_{l=-\infty}^{+\infty}\sum_{p=0}^{N_s^u-1}d_{p,l}c_{k,p,l}\right\} = \Re\left\{he^{j\tilde{\alpha}}\gamma\right\} \\ &= h\cos(2\pi\tilde{\alpha})\gamma_1 - h\sin(2\pi\tilde{\alpha})\gamma_2 = \mu_1\gamma_1 + \mu_2\gamma_2,\end{aligned} \tag{16}$$

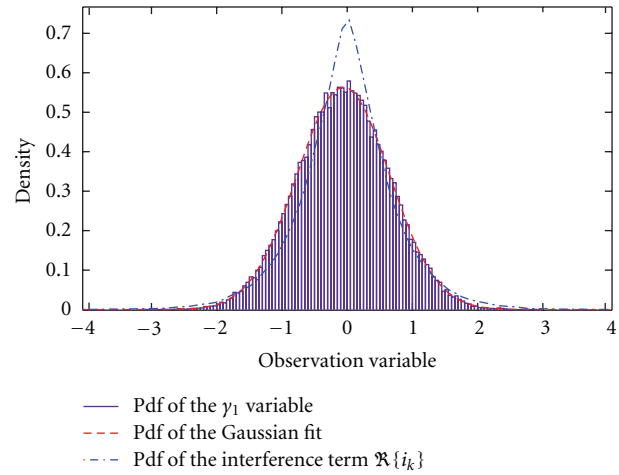

Figure 4: Probability distribution functions of the variables γ_1 and $\Re\{i_k\}$ both defined in (16).

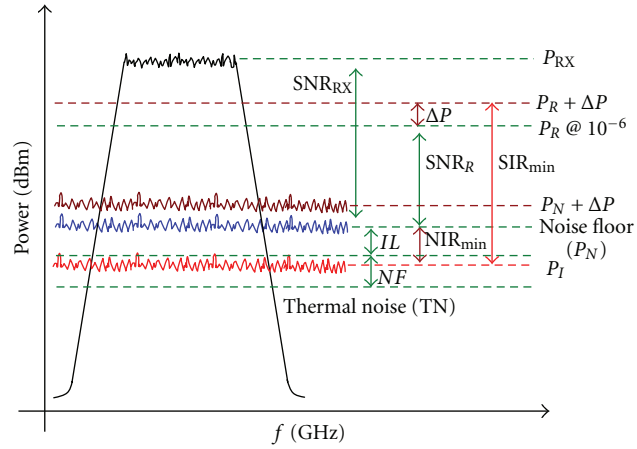

Figure 5: Power levels diagram for coexistence between WiMAX and MB-OFDM UWB Systems.

where the component $\gamma = \gamma_1 + j\gamma_2$ is a zero-mean complex Gaussian random variable with variance

$$\sigma_\gamma^2 = \sum_{l=-\infty}^{+\infty}\sum_{p=0}^{N_s^u-1}\left|c_{k,p,l}\right|^2, \tag{17}$$

as shown in Figure 4.

Furthermore, the random variables $\mu_1 = h\cos(2\pi\tilde{\alpha})$ and $\mu_2 = -h\sin(2\pi\tilde{\alpha})$ in (16) are zero-mean Gaussian distributed with variance $\sigma_{\mu_1}^2 = \sigma_{\mu_2}^2 = 1/2$, since h is a Rayleigh distributed variable that fulfils $\mathbb{E}\{h^2\} = 1$. Therefore, the CF of $\Re\{i_k\}$ conditioned to μ_1 and μ_2 is expressed as

$$\psi_{\Re\{i_k\}\mid\mu_1,\mu_2}(s) = e^{-s^2\sigma_\gamma^2(\mu_1^2+\mu_2^2)/4}, \tag{18}$$

where the following relationship $\sigma_{\gamma_1}^2 = \sigma_{\gamma_2}^2 = \sigma_\gamma^2/2$ is applied.

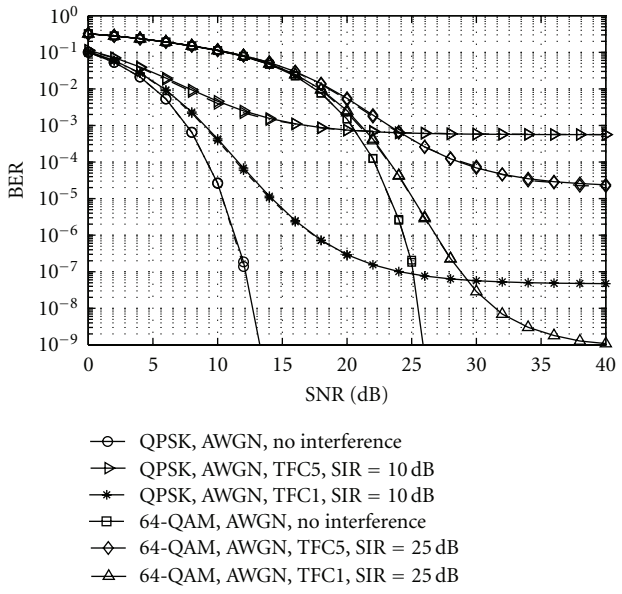

Figure 6: Analytical (continuous lines) and simulated (discontinuous lines) average BER versus $10\log 10(\text{SNR})$ for uncoded QPSK and 64-QAM WiMAX systems in an AWGN channel and with the presence of a single nonfaded MB-OFDM UWB interference with TFC1 and TFC5 frequency hopping patterns.

Finally, the expression of $\psi_{i_k}(s)$ is given by

$$\begin{aligned}\psi_{i_k}(s) &= \mathbb{E}_{|\mu_1,\mu_2}\left\{\psi_{\Re\{i_k\}|\mu_1,\mu_2}(s)\right\}\\ &= \int_{-\infty}^{+\infty} e^{(-s^2\sigma_y^2x^2)/4}\mathrm{P}_{\mu_1}(x)dx\int_{-\infty}^{+\infty} e^{(-s^2\sigma_y^2x^2)/4}\mathrm{P}_{\mu_2}(x)dx\\ &= \frac{1}{\sqrt{1+\left(s^2\sigma_y^2\sigma_{\mu_1}^2\right)/2}}\frac{1}{\sqrt{1+\left(s^2\sigma_y^2\sigma_{\mu_2}^2\right)/2}}\\ &= \frac{1}{1+\left(s^2\sigma_y^2\sigma_{\mu_1}^2\right)/2},\end{aligned} \tag{19}$$

where $\mathrm{P}_{\mu_1}(x)$ and $\mathrm{P}_{\mu_2}(x)$ are the probability density functions (pdf) of the Gaussian random variables μ_1 and μ_2, respectively.

Once the characteristic function of the decision variable r_k has been calculated, the BER for different modulation schemes can be computed. In the case of QPSK modulation, the threshold value in (10) is $d_{\tilde{x}_0} = 0$ and the BER expression for the subcarrier k can be simplified to

$$P_{k,\psi_{r_k}^{(m)}} = \frac{1}{2} + \frac{1}{2\pi}\int_0^{+\infty}\frac{\psi_{r_k}^{(m)}(-s) - \psi_{r_k}^{(m)}(s)}{js}ds. \tag{20}$$

When the chosen modulation scheme is M-QAM, the threshold value $d_{\tilde{x}_0}$ changes as a function of the distance between symbols. The BER value for M-QAM-based systems in AWGN is given in [22] and is extended in this work, when Rayleigh fading channel and MB-OFDM UWB interference are the distortive effects, to

$$\begin{aligned}P_{k,\psi_{r_k}^{(m)}} = {} & \frac{2}{\sqrt{M}\log_2\sqrt{M}}\sum_{k=1}^{F1}\sum_{i=0}^{F2}\left\{(-1)^{\lfloor(i2^{k-1})/\sqrt{M}\rfloor(2^{k-1})}\right\}\\ & -\left\lfloor\frac{i2^{k-1}}{\sqrt{M}}+\frac{1}{2}\right\rfloor\\ & \times\mathbb{P}\left(r_k < (2i+1)\sqrt{\frac{6\log_2 M}{2(M-1)}\frac{E_b}{N_0}}, \psi_{r_k}^{(m)}(s)\right),\end{aligned} \tag{21}$$

where $F1 = \log_2\sqrt{M}$, $F2 = 1 - 2^{-k}\log_2\sqrt{M} - 1$, and E_b is the energy of a transmitted bit.

Finally, the overall BER of the uncoded WiMAX system is obtained by distinguishing between two types of MB-OFDM UWB interference, frequency-hopped interference (TFC1) and nonhopping interference (TFC5). This results in

$$P_u = \frac{1}{3}\left(\frac{1}{N_s^w}\sum_{k=0}^{N_s^w-1}P_{k,\psi_{r_k}^{(m)}}\right) + \frac{2}{3}\left(\frac{1}{N_s^w}\sum_{k=0}^{N_s^w-1}P_{k,\psi_{r_k}^{(n)}}\right), \tag{22}$$

where $m = n = 1$ in the case of TFC5 and $m = 1$ and $n = 2$ for TFC1.

The BER expressions are represented as a function of the received signal-to-noise ratio (SNR) and SIR parameters, which are defined in this work as

$$\begin{aligned}\text{SNR} &= \frac{\mathbb{E}\left\{s_k^2\right\}}{\mathbb{E}\left\{2n_k^2\right\}} = \frac{\mathbb{E}\left\{G_k^2\right\}}{2\sigma_n^2} = \frac{P_S}{P_N},\\ \text{SIR} &= \frac{\mathbb{E}\left\{s_k^2\right\}}{\mathbb{E}\left\{2i_k^2\right\}} = \frac{P_S}{2\mathbb{E}\{h^2\}\mathbb{E}\left\{\sigma_y^2\right\}K_I},\end{aligned} \tag{23}$$

respectively. The index $k = 0,\ldots,N_d^w$ in (23) accounts for the data WiMAX subcarriers, P_S is the mean received power of the WiMAX signal, P_N is the noise power and the parameter K_I takes values 1/3 and 1 for TFC1 and TFC5 interference modes, respectively.

3.2. BER Performance for Coded WiMAX Systems. The BER expression of a system with convolutional coding of rate $R_{\text{cc}} = k_{\text{cc}}/n_{\text{cc}}$ is approximated, by truncating the union bound in [21, page 418], by

$$P_{\text{cc}} \le \frac{1}{k_{\text{cc}}}\sum_{d=d_f}^{d_f+N}\beta_d\text{PEP}(d), \tag{24}$$

where d_f is the free distance of the convolutional code, N is the truncating order, β_d is the weight spectrum of the code and $\text{PEP}(d)$ is the pairwise error probability, defined as the probability that the decoder erroneously selects a code sequence other than the transmitted one. The values of d_f and β_d are tabulated in [23, 24] for all the punctured codes.

Furthermore, the expression of $\text{PEP}(d)$ can be approximated by

$$\text{PEP}(d) \le [4P_u(1-P_u)]^{d_f/2}, \tag{25}$$

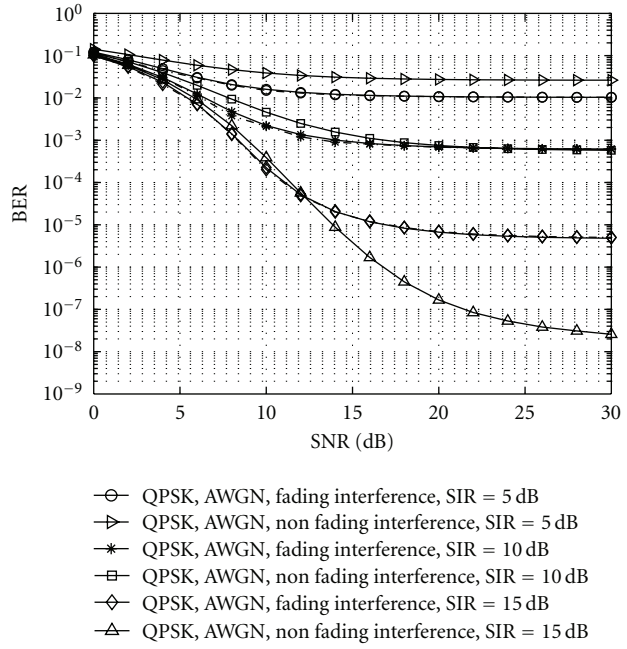

Figure 7: Analytical (continuous lines) and simulated (discontinuous lines) average BER versus $10\log 10(\text{SNR})$ for an uncoded QPSK WiMAX link in an AWGN channel and with the presence of a single nonfaded/Rayleigh-faded MB-OFDM UWB interference with TFC5.

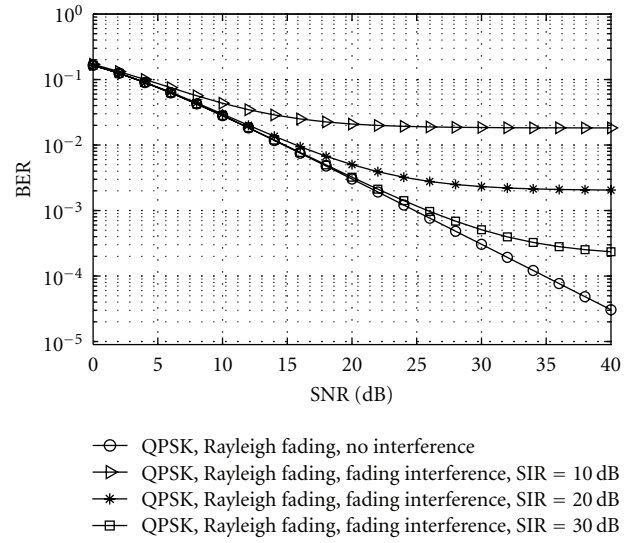

Figure 8: Analytical average BER versus $10\log 10(\text{SNR})$ for an uncoded QPSK WiMAX link in a Rayleigh fading channel and with the presence of a single Rayleigh-faded MB-OFDM UWB interference that follows a TFC5 pattern.

where P_u is the BER of the uncoded system given by equation (22), [25].

When the outer code is RS, the m-bit symbol error probability P_{sym} calculated at the output of the Viterbi decoder, can be obtained with a simple upper bound on P_{sym} as

$$P_{\text{sym}} \leq mP_{\text{cc}}, \tag{26}$$

where $m = \log_2(n_{\text{rs}} + 1)$ and $R_{\text{rs}} = k_{\text{rs}}/n_{\text{rs}}$ is the code rate of the RS encoder [26].

Finally, the symbol error probability P_{sym} is employed in the following equation to obtain the overall bound on the BER, calculated at the output of the RS decoder [21, page 473], as follows:

$$P_c < \frac{1}{n_{\text{rs}}} \sum_{i=T+1}^{n_{\text{rs}}} i\binom{n}{i} P_{\text{sym}}^i \left(1 - P_{\text{sym}}\right)^i, \tag{27}$$

where T is the error correction capability of the code.

3.3. Estimation of Interference Margins. In the context of the coexistence of WiMAX with MB-UWB OFDM, determining the maximum permissible interference level that maintains a satisfactory quality of service of the victim receiver, even in situations of minimum received power, is indispensable. Initially, it is important to identify the conditions under which the interference level is most harmful. This occurs when the WiMAX device, operating in DL mode, is located near the cell edge and the UWB interferer is in zone 1 of

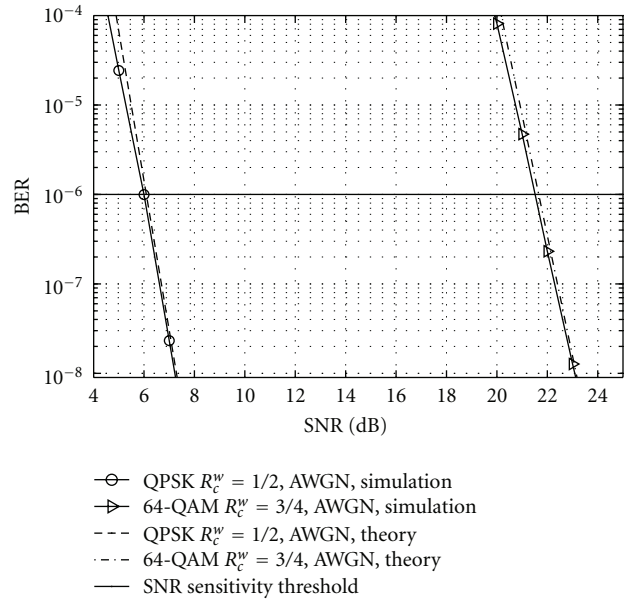

Figure 9: Analytical (discontinuous lines) and simulated (continuous lines) average BER versus $10\log 10(\text{SNR})$ for coded QPSK $R_c^w = 1/2$ and 64-QAM $R_c^w = 3/4$ WiMAX systems.

Figure 2. The IEEE 802.16 e standard specifies the minimum SNR, measured at the receiver input, required to obtain a BER value of 10^{-6} for each modulation-coding scheme in an AWGN channel. This value is defined as

$$\text{SNR}_R = \frac{\mathbb{E}_{|P_S=P_R}\left\{s_k^2\right\}}{\mathbb{E}\left\{2n_k^2\right\}} = \frac{P_R}{P_N}, \tag{28}$$

where P_R represents the WiMAX receiver sensitivity. The noise power measured in dBm units is given by

$$P_{N|\text{dBm}} = \text{TN} + 10\log_{10}(\text{BW}_e) + \text{NF} + \text{IL}, \tag{29}$$

where TN is the thermal noise spectral density in dBm/Hz units, BW_e is the effective bandwidth, NF is the noise figure in dB and IL models the implementation losses in dB units. The TN value is computed as the product of the Boltzmann's constant and the room temperature. Considering an ambient temperature of 290 K, a normalized TN $= -174$ dBm/Hz is obtained. The effective channel bandwidth can be calculated from

$$\text{BW}_e = \frac{N_d^w f_s}{N_s^w R_c^w}, \tag{30}$$

where $f_s = n\text{BW}$ is the nominal bandwidth of the WiMAX signal. The values of NF and IL are commonly set to 7 dB and 5 dB, respectively, and these values are used in this work.

In the presence of MB-OFDM UWB interference, it is expected that the minimum required WiMAX receiver sensitivity, and therefore the SNR_R, will increase for any power level of the interference. However, it is of paramount interest to estimate the maximum tolerable interference level in order to evaluate the correct behavior of the DAA algorithm. In this paper, the parameter employed to analyze the interference effects is the signal-to-interference ratio. The SIR value measured at the minimum received sensitivity is expressed as

$$\text{SIR}_{\min} = \frac{P_R \Delta P}{P_I} = \frac{\mathbb{E}\left\{s_k^2\right\}\Delta P}{\mathbb{E}\left\{2i_k^2\right\}} = \frac{\mathbb{E}\left\{G_k^2\right\}\Delta P}{2\sigma_v^2\sigma_q^2}, \tag{31}$$

where P_I is the received power of the MB-OFDM UWB interference signal and ΔP models the increase of the receiver sensitivity due to the addition of the interference signal.

The power levels of the WiMAX/UWB coexistence system are shown in Figure 5. By setting the value of the maximum interference power level allowed at the WiMAX receiver $P_{I|\max}$ to the DAA levels, the expression of the minimum required SIR can be computed as

$$\text{SIR}_{\min} = \frac{\text{SNR}_R \Delta P P_N}{P_{I|\max}} = \text{SNR}_R \Delta P \text{NIR}_{\min}, \tag{32}$$

where $\text{NIR}_{\min}$ is the minimum allowed noise-to-interference ratio value. It is stipulated in the IEEE 802.16e standard [3] that $P_{I|\max} = P_N$. Also, the MB-OFDM UWB interference can be modeled as a Gaussian noise due to the noise-like amplitude variability of the OFDM-based signal [14]. Under these conditions, the maximum tolerable increment of receiver sensitivity ΔP is approximately 3 dB, and the relationship $\text{SIR}_{\min} = \text{SNR}_R \Delta P$ is obtained.

The received interference power level, P_I, can be computed by means of a link budget analysis. The propagation conditions considered in this work correspond to the case of free-space propagation loss which is calculated, using Frii's formula, as

$$P_I = \frac{P_U G_T G_R}{L_p}, \tag{33}$$

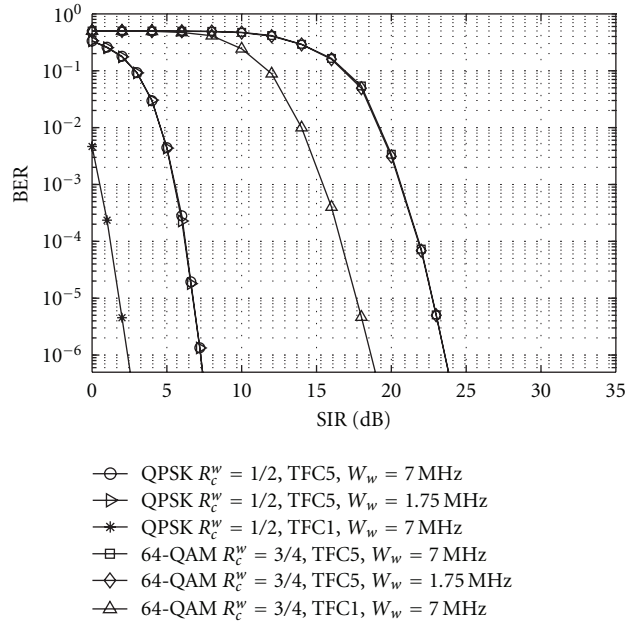

Figure 10: Average BER versus $10\log 10(\text{SIR})$ for QPSK $R_c^w = 1/2$ and 64-QAM $R_c^w = 3/4$ WiMAX systems in TFC5 and TFC1 mode and SNR $\to \infty$. Two different WiMAX bandwidths are considered: $W_w = 1.75$ MHz and $W_w = 7$ MHz.

where G_T and G_R are the antenna gains of the UWB transmitter and the WiMAX receiver, respectively, and L_p is the path loss with value $L_p = (4\pi f_u d/c)^2$. The parameters c and d are the speed of light and the distance between the UWB interferer and the WiMAX receiver.

Finally, the minimum distance value between victim service and the interferer can be calculated by substituting (29) and (33) into the expression $P_N = \text{NIR}_{\min} P_{I|\max}$, yielding

$$d_{\min} = \frac{c}{4\pi f_u}\sqrt{\frac{P_U G_T G_R \text{NIR}_{\min}}{P_N}}. \tag{34}$$

Furthermore, the distance values, that delimit the zones in the DAA mechanism of Figure 2, can be calculated by using (34). As an example of this application, a WiMAX system with 64-QAM $R_c^w = 3/4$ scheme, nominal bandwidth of $f_s = 2$ MHz and $G_T = G_R = 0$ dBi is considered. In this situation, the two threshold areas of the DAA algorithm are established by setting $d_{\min|z_1} = 0.68$ m and $d_{\min|z_2} = 14.78$ m for $\text{NIR}_{\min} = 2$ dB.

4. Numerical and Simulation Results

In this section, a comprehensive analysis of the MB-OFDM UWB interference effects on the WiMAX receiver is carried out by means of numerical and simulation methods. Initially, the analytical BER expressions for uncoded and coded WiMAX systems are validated through simulations in Section 4.1. Thereafter, simulated BER and EVM performances, provided in Section 4.2, allow the estimation

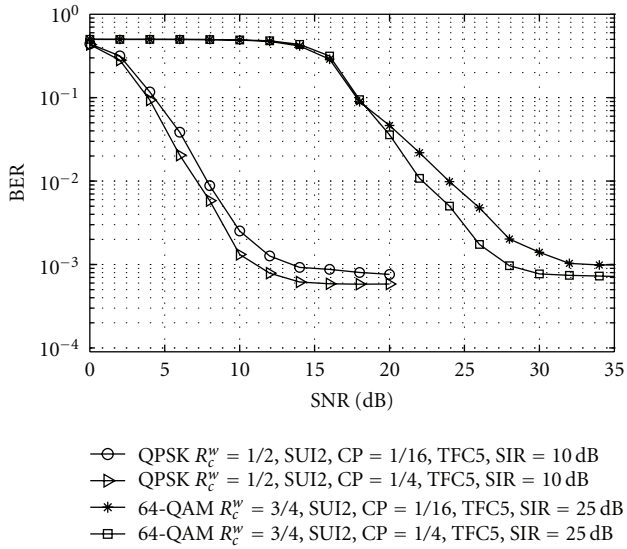

Figure 11: Average BER versus 10 log 10(SNR) for QPSK $R_c^w = 1/2$ and 64-QAM $R_c^w = 3/4$ WiMAX systems in TFC5 and multipath fading channel SUI-2.

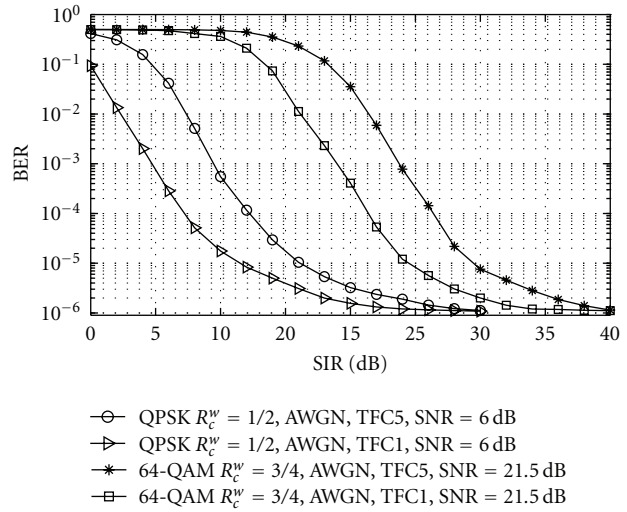

Figure 12: Average BER versus 10 log 10(SIR) for QPSK $R_c^w = 1/2$ and 64-QAM $R_c^w = 3/4$ WiMAX systems in TFC5 and TFC1 modes. The SNR is set to SNR_R.

of the maximum permissible interference levels. The main numerical values for both WiMAX and MB-OFDM UWB interferer systems employed in this study are summarized in Table 1.

4.1. Validation of Analytical BER Expressions. Initially, the analytical BER expressions for the uncoded WiMAX systems, obtained in section Section 3.1, are validated by means of numerical and simulation results. Firstly, the BER curves for uncoded WiMAX systems with QPSK and 64-QAM modulation schemes in the situation of AWGN channel and

Table 1: WiMAX and MB-OFDM main parameters.

WiMAX	
Parameters	Values
N_s^w	256
f_w	3.5 GHz
W_w	{1.75, 7, 17.5} MHz
T_w	$256/W_w$
T_{cp}^w	$\{0, 1/4, 1/16\}T_w$
T_s^w	$\{1, 5/4, 17/16\}T_w$
$R_{\mathrm{cc}} = k_{\mathrm{cc}}/n_{\mathrm{cc}}$	2/3 (QPSK 1/2)
	5/6 (64-QAM 3/4)
β_d	[3, 70, 285, 1276, 6160, 27128, 117019] (QPSK 1/2)
	[92, 528, 8694, 79453, 792114, 7375573] (64-QAM 3/4)
d_f	6 (QPSK 1/2)
	4 (64-QAM 3/4)
RS $(n_{\mathrm{rs}}, k_{\mathrm{rs}}, T)$	RS(32,24,4) (QPSK 1/2)
	RS(120,108,6) (64-QAM 3/4)
MB-OFDM UWB	
Parameters	Values
N_s^u	128
f_u	$2904 + i528$ MHz; $i = 1$ (TFC5), $i = \{1, 2, 3\}$ (TFC1)
W_u	528 MHz
T_u	242.42 ns
T_{cp}^u	70.07 ns
T_s^u	312.5 ns
R_b^u	200 Mbps

nonfaded MB-OFDM UWB interference signals are plotted in Figure 6. For comparison purposes, the simulated and numerical BER waterfall curves of these WiMAX systems without presence of interference are also represented in Figure 6. In this scenario, the CF of the nonfaded interference, calculated in (19), is replaced by the Gaussian CF expression $\psi_{i_k}(s) \approx \exp(-s^2\sigma_\gamma^2/2)$, since $\mu_1 = \mu_2 = 1$. The results illustrate that simulated BER curves are identical to the analytical results.

Secondly, the BER curves of a WiMAX system with QPSK modulation, in the presence of Rayleigh-amplitude faded interference with TFC5 hopping pattern, are depicted in Figure 7 for different SIR levels. The BER curves with faded interference are compared to those with nonfaded interference. The numerical results show that when the SIR is low (SIR = 5 dB and SIR = 10 dB), the faded interference improves the BER performance, with respect to the nonfaded interference case, since the pdf of the faded interference has larger values at the origin than the Gaussian pdf, as shown in Figure 4. However, the tails of the faded interference pdf display a larger amount of energy than the Gaussian pdf, causing a degradation of the BER performance when the SIR levels are high (SIR = 15 dB). In this scenario, the numerical BER curves also perfectly match the simulation results.

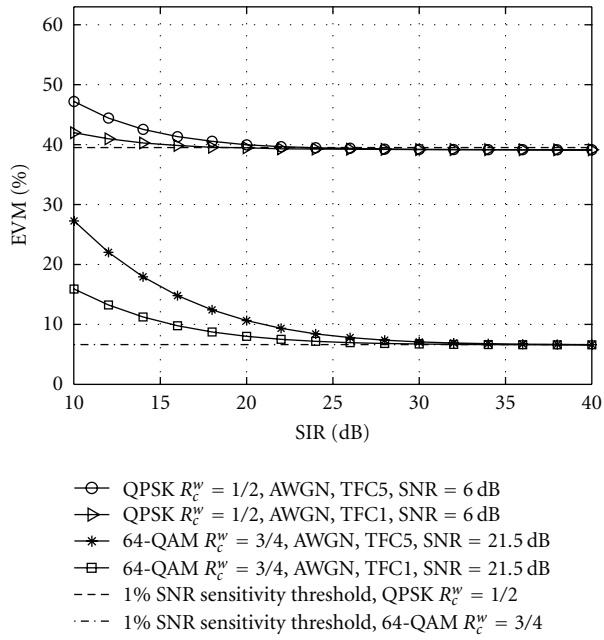

Figure 13: Percentage EVM versus $10\log 10(\text{SIR})$ for QPSK R_c^w = 1/2 and 64-QAM R_c^w = 3/4 WiMAX systems in TFC5 and TFC1 modes. The SNR is set to SNR_R and two threshold values are plotted following the 1% criterion.

Furthermore, the numerical and simulated BER expressions of the QPSK modulated WiMAX link, impaired by faded interference and Rayleigh fading, are plotted in Figure 8 for different values of the SIR. The simulated BER curves validate the theoretical analysis presented in Section 3.1.

Finally, the BER performance of the analytical upper bound coded WiMAX systems, using the burst profiles QPSK R_c^w = 1/2 and 64-QAM R_c^w = 3/4, are validated by means of simulation results, as shown in Figure 9. The simulation and numerical results are obtained by considering an AWGN channel and an interference-free scenario. The improvement in BER performance, resulting from the addition of the concatenated RS-CC coding to both systems with respect to the uncoded systems, is clearly manifested for high values of SNR. The required values of SNR, that guarantee a BER value of 10^{-6}, are obtained from Figure 9 as SNR_R = 6 dB and SNR_R = 21.5 dB for QPSK R_c^w = 1/2 and 64-QAM R_c^w = 3/4, respectively. These values will be employed for estimating the interference levels in further analysis. It is noticeable that the analytical upper bound BER performances are in agreement with the simulated waterfall BER curves for large SNR values.

4.2. Simulation Results: Evaluation of Interference Effects. The average BER performances, as a function of the received SIR of the two modulation-coding WiMAX systems, are plotted in Figure 10 for both frequency-hopped (TFC1) and fixed (TFC5) types of interference. In order to correctly assess the effect of the interference signal on the victim service, as the only source of distortion, the AWGN noise contribution is considered negligible in this simulation scenario (SNR $\rightarrow \infty$).

Initially, it is noticeable that the BER of the TFC5 interference systems degrades by approximately 4.5 dB with respect to the TFC1 systems. This is due to the fact that only one third of the UWB interference symbols with TFC1 frequency hopping pattern cause interference to the WiMAX link. The Gaussian behavior of the interference can also be observed in this analysis. The BER waterfall curves of the TFC5 interference systems are almost identical to the noninterference coded BER curves, represented in Figure 9, but shifted approximately 1.5 dB. This is due to the larger value of the interference variance.

Two WiMAX systems with transmission bandwidth values W_w = 7 MHz and W_w = 1.75 MHz are used in this initial analysis. The BER performances of these systems, plotted in Figure 10 for the case of TFC5, are shown to be practically identical, leading to the conclusion that the MB-OFDM UWB interference effects on an IEEE 802.16-2004 WiMAX system in an AWGN channel is independent of its subcarrier spacing. It was shown in [15] that the BER performance of a WiMAX system degrades as the subcarrier separation of the UWB interferer decreases. However, in the inverse situation, in which the subcarrier separation of the interference is fixed to Δf_u = 4.125 MHz, the interference distortion on WiMAX systems with W_w = 7 MHz (Δf_w = 27.34 KHz) and W_w = 1.75 MHz (Δf_w = 6.83 KHz) behaves the same since only very few UWB subcarriers contribute to the interference component within the narrow WiMAX bandwidth.

In the following analysis, a more realistic simulation environment is applied by considering a multipath fading channel. The radio channel is based on the Stanford University Interim (SUI) channels for fixed broadband wireless access systems [27]. The SUI model is a set of six channels that characterize the impulse response for three different types of terrains, considering the mobility of the user by means of the Doppler spread parameter. Each SUI multipath channel is obtained by defining three taps with the corresponding power, delay spread, and K-factor. In this set of simulations, SUI-2 channel (which accounts for low delay spread and low Doppler spread values) is considered for evaluating the BER performance of the WiMAX systems with W_w = 17.5 MHz impaired by TFC5 interference signals, as illustrated in Figure 11. In this simulation study, SIR = 10 dB and SIR = 25 dB are set for QPSK R_c^w = 1/2 and 64-QAM R_c^w = 3/4, respectively. The resulting BER simulations show the degradation of performance when using a short cyclic prefix of CP = 1/16 with respect to a long prefix of CP = 1/4. This performance degradation is caused by the fact that the excess delay D_w = 1 μs of the three-path SUI-2 channel is larger than T_{cp}^w = 0.9 μs when CP = 1/16. In contrast, the excess delay is less than T_{cp}^w = 3.7 μs when CP = 1/4 is employed. It can also be observed that the BER curves tend to a particular floor value for high SNR, which is determined by the fixed SIR levels.

Finally, the estimation of the maximum allowable interference levels and the SIR levels that allow the interference signal to be considered negligible are obtained by means of simulations in the following analysis. The BER performances, as a function of the received SIR for the two

burst profiles with fixed received SNR values, are plotted in Figure 12. In this study, the WiMAX bandwidth is set to $W_w = 7$ MHz and MB-OFDM UWB interferers employ both TFC1 and TFC5 hopping patterns. The received SNR values are chosen as those that guarantee a BER $= 10^{-6}$ in AWGN channel conditions (SNR_R), which are obtained in Figure 9 and correspond to 6 dB and 21.5 dB for QPSK $R = 1/2$ and 64-QAM $R = 3/4$, respectively. As previously mentioned in the analytical approach (Section 3.3), the maximum permissible UWB interference level is set to the noise floor, yielding $\text{SIR}_{\min} = \text{SNR}_R + 3$ dB in (32). In this situation, the BER performance degrades considerably with respect to the case of noninterference, especially when TFC5 is employed, obtaining BER values of approximately $1 \cdot 10^{-3}$ and $5 \cdot 10^{-5}$ for QPSK $R_c^w = 1/2$ and 64-QAM $R_c^w = 3/4$, respectively. Therefore, a more precise approach must be adopted for neglecting the interference. It is stipulated in [28] that an interference signal can be neglected when its effects on the measured metrics are $\leq 1\%$.

The SIR values that are compliant with the 1% criterion can be obtained in a more accurate manner by analyzing the EVM performance instead of the BER. The EVM is a baseband system-level metric that allows the quality of the system to be evaluated by calculating the error in the constellation diagram. Also, the computation of the EVM metric is faster and less complex to obtain in both simulation and experimental studies. The EVM performance of the two coded systems are represented in Figure 13 under the same scenario as previously indicated. The percentage of EVM of a QPSK $R_c^w = 1/2$ system, in AWGN without interference when operating at its minimum sensitivity ($\text{SNR}_R = 6$ dB), is calculated as 39.15%. Similarly, a percentage EVM of 6.55% is required for 64-QAM $R_c^w = 3/4$ with $\text{SNR}_R = 21.5$ dB. By applying a 1% factor to these values, the two thresholds are obtained, as shown in Figure 13. Under these conditions and using the 1% criterion, it can be concluded that the SIR values for noninterference coexistence operability (SIR_{IF}) are 19 dB and 23.5 dB for QPSK $R_c^w = 1/2$ with TFC1 and TFC5, respectively. For 64-QAM $R_c^w = 3/4$, the SIR_{IF} values are 32 dB and 36.5 dB for TFC1 and TFC5, respectively.

5. Experimental Results

The objective of the measurement analysis is to estimate the interference margin levels, $\text{SIR}_{\min}$ and SIR_{IF}, in order to validate the results previously obtained in the simulation study. Initially, the laboratory test bed, implemented for the measurement campaign, is described in Section 5.1. Subsequently, measurement results given by EVM and SEP metrics are provided in Section 5.2 for different types of interference scenarios.

5.1. Laboratory Test Bed Description. The laboratory test bed for coexistence study between WiMAX and MB-OFDM UWB in the conducted modality is depicted in Figure 14. The instruments employed are listed as follows.

(i) WiMAX baseband vector signal generator (Rohde & Schwarz SMBV100A). Upconverter: Agilent PSG E8267D.

(ii) WiMAX Receiver: Tektronix Real-Time Spectrum Analyzer RSA3408B.

(iii) WiMAX Demodulator: WiMAX IQSignal software application running on a stand-alone pc.

(iv) Two UWB MB-OFDM Sources: (1) Tektronix AWG7000B UWB Signal Generator. (2) Wisair DV9110 WiMedia evaluation system operating in the test mode connected to a variable attenuator (0–69 dB).

(v) Signal combiner.

This test bed has been designed to monitor the errors in the WiMAX channel for any arbitrary values of SNR and SIR. The test bed has the advantage of employing a realtime spectrum analyzer as a programmable WiMAX receiver. Therefore, full control of the receiver parameters, such as center frequency, bandwidth, sampling frequency, and external triggering, is achieved. Also, it allows the use of a WiMAX demodulator software that provides a quantitative estimation of the interference impact on the WiMAX receiver. However, the noise figure of the spectrum analyzer is poorer than the state of the art WiMAX receiver and this difference needs to be taken into account in the measurements. An estimated noise floor of the spectrum analyzer of -84 dBm/MHz is obtained, which is approximately 20 dB poorer than a typical state of the art WiMAX receiver. Furthermore, the analog-to-digital conversion in the spectrum analyzer is made with 16-bits and, therefore, the receiver has a dynamic above 90 dB. This can be significantly increased using the auto range functionality that sets an adaptive level of the reference signal.

5.2. Measurement Results. Initially, the performance of the two burst profile WiMAX systems, QPSK $R_c^w = 1/2$ and 64-QAM $R_c^w = 3/4$, is evaluated in an AWGN channel without the presence of interference in order to obtain a performance benchmark for the measurement setup. The EVM performances, as a function of the received SNR, are illustrated in Figure 15(a) for WiMAX systems with $W_w = 7$ MHz. Each plotted curve corresponds to an extensive series of 250 measurements, since 25 different power levels ranging from -80 to -25 dBm have been used, and each measured value is obtained from averaging 10 measurement realizations. This procedure is applied for all the measurements performed in this work. The measurement results show that the minimum SNR values, that guarantee a WiMAX channel free of errors (i.e., sensitivity of the receiver), are approximately 6 dB and 22 dB for QPSK $R_c^w = 1/2$ and 64-QAM $R_c^w = 3/4$, respectively. These SNR_R values are in agreement with those obtained in the simulation analysis in Section 4.2. Note that symbol errors are represented by black-filled markers in the graphical representations.

An interference scenario with a dominant MB-OFDM UWB interference signal, whose power level is significantly larger than the thermal noise in the WiMAX channel, is

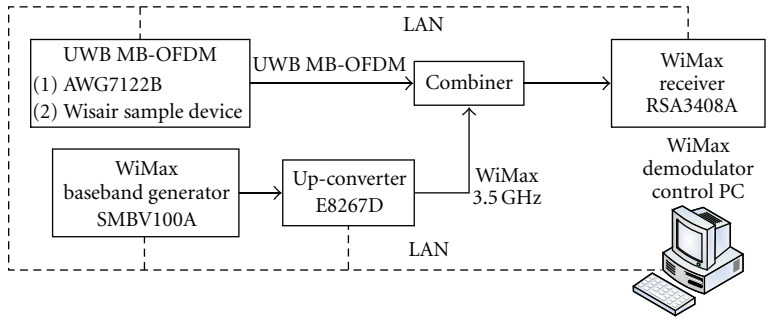

Figure 14: Laboratory setup for conducted tests.

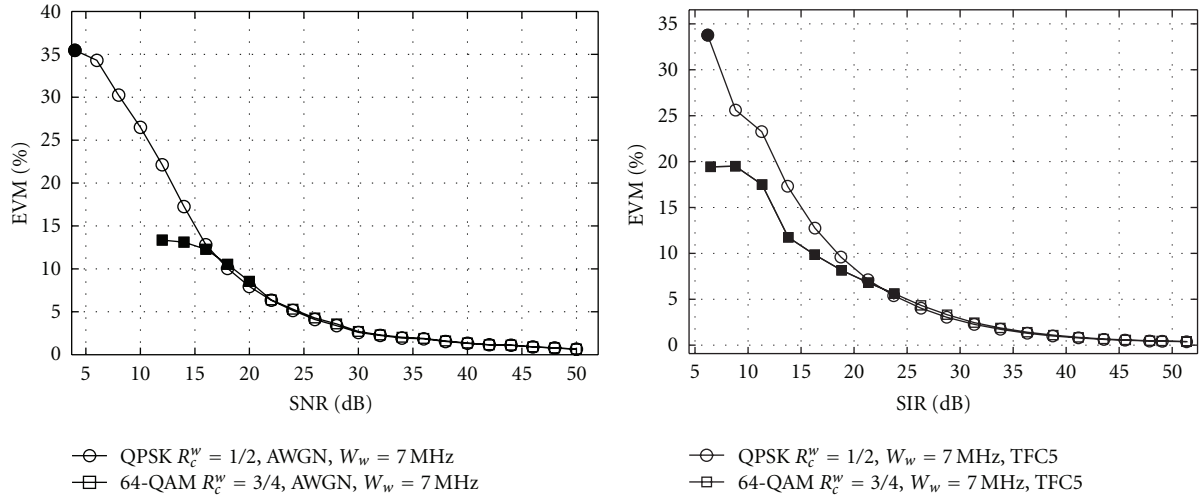

(a) %EVM versus 10 log 10 (SNR)

(b) %EVM versus 10 log 10 (SNR)

Figure 15: Measured percentage EVM performances for QPSK $R_c^w = 1/2$ and 64-QAM $R_c^w = 3/4$. (a) Interference-free scenario. (b) TFC5 Interference with NIR = 11 dB.

considered in the following analysis. The MB-OFDM UWB interference signals, with $R_b = 200$ Mbps and power spectral density (PSD) of -73 dBm/Mhz, are generated from the AWG7112B signal generator for TFC5 frequency-hopping pattern. This PSD value is 11 dB larger than the noise floor. The measurement campaign is carried out in the worst possible interfering scenario, which corresponds to a duty cycle of the interference signal of 100%. The average received EVM performances for the two burst profiles under these interference conditions are shown in Figure 15(b). The results illustrate that the WiMAX receiver with concatenated RS-CC coding is not capable of successfully demodulating the symbols when the SIR level is very low for TFC5 interference signalling. In particular, there are symbol errors when SIR $\leq$ 8 dB and SIR $\leq$ 24 dB for QPSK $R = 1/2$ and 64-QAM $R = 3/4$, respectively. For larger values of the SIR, the measured EVM values are the same for both burst profiles and slightly larger than those without interference and AWGN noise.

Finally, a set of conducted measurements employing the WiMedia sample device (i.e., a Wisair DV9110 WiMedia evaluating system operating in the test mode) with TFC5 and a WiMAX link, with 64-QAM $R_c^w = 3/4$ scheme, are carried out in the following analysis. In order to conveniently adjust the output power of the UWB sample device, a variable attenuator is employed. The level of the interfering signal is selected to obtain interference-to-noise (INR) levels between 2 dB and -11 dB. The objective here is to estimate the value of SIR_{IF} for the situation of neglected interference. In the test mode, this sample device operates with a fixed duty cycle of 50%, a frame duration of 600 μs and a constant data rate of 200 Mbps. The measurement results illustrate that the effects of the interference signal become negligible when NIR $\geq$ 10 dB, as shown in Figure 16(a) when EVM is the measured metric and in Figure 16(b) for the symbol error probability (SEP) analysis. This NIR limit value corresponds to an EVM of -24 dB (i.e., 6.31 of %EVM). This value is in agreement with the simulated threshold for 64-QAM $R_c^w = 3/4$ obtained in Section 4.2. Thus, the measurement results validate the SIR_{IF} values obtained by simulations.

6. Conclusions

New EIRP masks released by the European Commission in its Decision 2007/131/EC regulate the radio spectrum use for UWB equipment in the European Community.

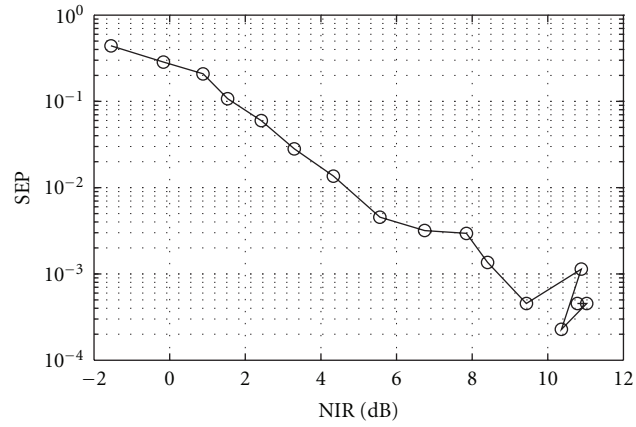

(a) %EVM versus 10 log 10 (NIR)

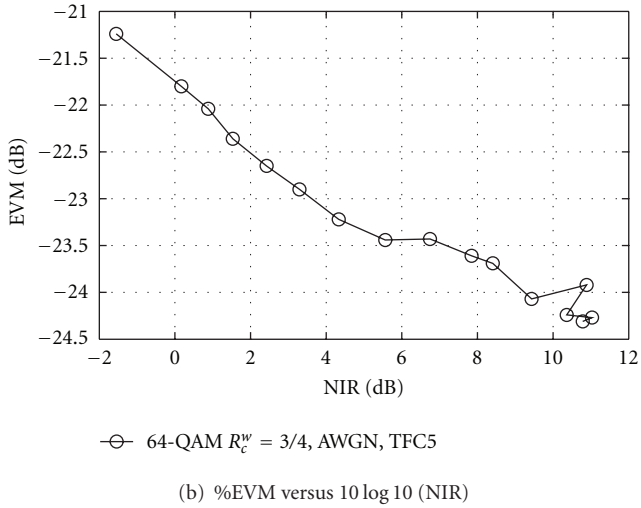

(b) %EVM versus 10 log 10 (NIR)

Figure 16: Measured EVM and SEP performances for 64-QAM R_c^w = 3/4 WiMAX systems in the presence of an MB-OFDM UWB interference in TFC5 mode.

In particular, UWB devices are required to use interference mitigation techniques in order to coexist with licensed BWA systems, such as WiMAX at 3.5 GHz, without causing harmful interference. The DAA mechanism, based on the definition of three zones of operation, dynamically allocates the power of the UWB devices by sensing the presence of WiMAX activity.

The objective of this work is to evaluate the performance of the WiMAX victim receiver under the presence of a single MB-OFDM UWB interferer with DAA capabilities. In the context of interference, a WiMAX receiver, operating in DL at its minimum sensitivity level impaired by an MB-OFDM UWB active interferer located in Zone 1 of the DAA protection area, was identified as the most critical scenario. A comprehensive analysis of these interference effects has been provided in this paper by means of theoretical, simulation and measurement approaches.

Novel analytical expressions of the BER for uncoded and coded WiMAX systems, impaired by a single MB-OFDM UWB interference signal, were provided in this paper for both AWGN and Rayleigh fading channel environments. The BER expressions were obtained by applying the inversion theorem, which expresses the BER as a function of the characteristic function of the decision variable. In this approach, the complexity associated with calculating the exact BER is reduced by first computing the characteristic function of the received interference contribution. Furthermore, the maximum allowable interference levels SIR_{min} were analytically obtained.

An extensive simulation analysis has been provided in this paper. Initially, the analytical BER expressions for uncoded QPSK and 64-QAM WiMAX systems, in the presence of a MB-OFDM UWB interference signals, were validated through simulations for different scenarios. Furthermore, the upper bound analytical BER expressions for coded QPSK $R_c^w = 1/2$ and 64-QAM $R_c^w = 3/4$ were also validated through simulations. Subsequently, the simulation results showed that the effect of the nonhopping UWB interference on the WiMAX link is 4.5 dB larger than the hopping one. This is due to the fact that the frequency-hopped interference is only active one third of the time. The Gaussian behavior of the MB-OFDM UWB interference was also illustrated in the simulation analysis. Furthermore, it was shown that the MB-OFDM UWB interference effects on an IEEE 802.16-2004 WiMAX system in an AWGN channel is independent of its subcarrier spacing.

The simulation results also showed the effects of the intersymbol interference caused by selecting a short cyclic prefix length of the WiMAX signal in a multipath channel environment.

This simulation study allowed the BER values for $\text{SIR} = \text{SIR}_{\text{min}}$ to be graphically measured. In this situation, the results showed that the BER degrades considerably with respect to the case of noninterference, especially when TFC5 is employed. More restrictive SIR levels are required in order to neglect the UWB interference effects. The 1% criterion was employed on the EVM performance to estimate the SIR_{IF} levels. It has been demonstrated that the SIR values for noninterference coexistence operability are 19 dB and 23.5 dB for QPSK $R_c^w = 1/2$ with TFC1 and TFC5, respectively. For 64-QAM $R_c^w = 3/4$, the SIR_{IF} values are 32.5 dB and 36.5 dB for TFC1 and TFC5, respectively.

Measurements in a conducted modality have been carried out to analyze the effects of the UWB interference on the WiMAX link for two defined situations. Firstly, the UWB interference level is larger than the noise floor allowing SIR_{min} levels, with no symbol errors in the demodulation process, to be set. Secondly, the UWB interference is of the order of the noise floor and the WiMAX receiver operates at its minimum sensitivity level. In this situation, it is concluded that the effects of the interference signal become negligible when the NIR is larger than 10 dB.

References

[1] D. Porcino and W. Hirt, "Ultra-wideband radio technology: potential and challenges ahead," *IEEE Communications Magazine*, vol. 41, no. 7, pp. 66–74, 2003.

[2] IEEE Std. 802.16-2004, "IEEE Standard for Local and Metropolitan Area Networks, Part 16: Air Interface for Fixed

and Mobile Broadband Wireless Access Systems," October 2004.

[3] IEEE Std. 802.16e-2005, "IEEE Standard for Local and Metropolitan Area Networks, Part 16: Air Interface for Fixed and Mobile Broadband Wireless Access Systems, Amendment for Physical and Medium Access Layers for Combined Fixed and Mobile Operation in Licensed Bands," February 2006.

[4] Federal Communications Commission (FCC), "Revision of Part 15 of the Commissions Rules Regarding Ultra-Wideband Transmission Systems," First Report and Order ET Docket 98-153, FCC 02-48, April 2002.

[5] European Commission Decision 2007/131/EC, "Allowing the Use of the Radio Spectrum for Equipment Using Ultra-Wideband Technology in a Harmonised Manner in the Community," June 2007.

[6] ECC Repot 120, "Technical Requirements for UWB DAA (Detect and Avoid) Devices to Ensure the Protection of Radiolocation in the Bands 3.1–3.4 GHz and 8.5–9 GHz and BWA Terminals in the Band 3.4–4.2 GHz," February 2007.

[7] A. Batra, J. Balakrishnan, G. R. Aiello, J. R. Foerster, and A. Dabak, "Design of a multiband OFDM system for realistic UWB channel environments," *IEEE Transactions on Microwave Theory and Techniques*, vol. 52, no. 9 I, pp. 2123–2138, 2004.

[8] S. M. Mishra, S. ten Brink, R. Mahadevappa, and R. W. Brodersen, "Cognitive technology for ultra-wideband/WiMax coexistence," in *Proceedings of the 2nd IEEE International Symposium on New Frontiers in Dynamic Spectrum Access Networks*, pp. 179–186, April 2007.

[9] A. Rahim, S. Zeisberg, and A. Finger, "Coexistence study between UWB and WiMax at 3.5 GHz band," in *Proceedings of IEEE International Conference on Ultra-Wideband (ICUWB '07)*, pp. 915–920, September 2007.

[10] F. Facchini, R. Giuliano, and F. Mazzenga, "Ultra-wideband detect and avoid procedure for WiMAX victims," *IET Communications*, vol. 3, no. 2, pp. 268–278, 2009.

[11] A. Durantini, R. Giuliano, F. Mazzenga, and F. Vatalaro, "Performance evaluation of detect and avoid procedures for improving UWB coexistence with UMTS and WiMAX systems," in *Proceedings of IEEE International Conference on Ultra-Wideband (ICUWB '06)*, pp. 501–506, September 2006.

[12] R. Kogane, C. Fukao, J. Hioki et al., "A study on the detection scheme of WiMAX signal for DAA operation in MB-OFDM," in *Proceedings of IEEE International Conference on Ultra-Wideband (ICUWB '07)*, pp. 834–839, September 2007.

[13] J. Perez, M. Beltrán, M. Morant, R. Llorente, and L. Cavallin, "Protection margins for joint operation of WiMAX 802.16e and WiMedia-defined UWB radio in personal area networks," in *Proceedings of IEEE International Conference on Ultra-Wideband (ICUWB '09)*, pp. 723–727, Vancouver, Canada, September 2009.

[14] K.-W. Kim, J. Park, J. Cho et al., "Interference analysis and sensing threshold of detect and avoid (DAA) for UWB coexistence with WiMax," in *Proceedings of the 66th IEEE Vehicular Technology Conference (VTC '07)*, pp. 1731–1735, October 2007.

[15] A. Nasri, R. Schober, and L. Lampe, "Performance evaluation of BICM-OFDM systems impaired by UWB interference," in *Proceedings of IEEE International Conference on Communications (ICC '08)*, pp. 3616–3621, May 2008.

[16] C. Snow, L. Lampe, and R. Schober, "Error rate analysis for coded multicarrier systems over quasi-static fading channels," *IEEE Transactions on Communications*, vol. 55, no. 9, pp. 1736–1746, 2007.

[17] C. Snow, L. Lampe, and R. Schober, "Analysis of the impact of WiMAX-OFDM interference on multiband OFDM," in *Proceedings of IEEE International Conference on Ultra-Wideband (ICUWB '07)*, pp. 761–766, September 2007.

[18] European Computer Manufacters Association (ECMA), "Standard ECMA-368: High Rate Ultra Wideband PHY and MAC Standard," December 2005.

[19] O. Edfors, M. Sandell, J. van de Beek, D. Landstrom, and F. Sjoberg, "An introduction to orthogonal frequency-division multiplexing," Research Report, 1996, http://www.sm.luth.se/csee/sp/publications/.

[20] J. Gil-Pelaez, "Note on the inversion theorem," *Biometrika*, vol. 38, no. 3/4, pp. 481–482, 1951.

[21] J. G. Proakis, *Digital Communications*, McGraw-Hill, New York, NY, USA, 5th edition, 2008.

[22] D. Yoon, K. Cho, and J. Lee, "Bit error probability of M-ary quadrature amplitude modulation," in *Proceedings of the 52nd Vehicular Technology Conference (VTC '00)*, vol. 5, pp. 2422–2427, September 2000.

[23] D. Haccoun and G. Begin, "High-rate punctured convolutional codes for Viterbi and sequential decoding," *IEEE Transactions on Communications*, vol. 37, no. 11, pp. 1113–1125, 1989.

[24] P. Frenger, P. Orten, and T. Ottosson, "Convolutional codes with optimum distance spectrum," *IEEE Communications Letters*, vol. 3, no. 11, pp. 317–319, 1999.

[25] R. D. Wessel, "Convolutional codes," in *Wiley Encyclopedia of Telecommunications*, J. G. Proakis, Ed., vol. 1, pp. 598–606, John Wiley & Sons, Hoboken, NJ, USA, 2003.

[26] M.-O. Wessman, A. Svensson, and E. Agrell, "Frequency diversity performance of coded multiband-OFDM systems on IEEE UWB channels," in *Proceedings of the 60th IEEE Vehicular Technology Conference (VTC '04)*, pp. 1197–1201, September 2004.

[27] V. Erceg, et al., "Channel Models for Fixed Wireless Applications," IEEE 802.16.3c-01/29rl, February 2001.

[28] ECC Report 64, "The Protection Requirements of Radiocommunications Systems Below 10.6 GHz from Generic UWB Applications," February 2005.